

## Electrochemical Corrosion Behaviour of X70 Steel in Zinc ( II)-Contaminated Sand Soil

Pengju Han<sup>1,2</sup>, Ruizhen Xie<sup>1\*</sup>, Run Liu<sup>2\*</sup>, Bin He<sup>1</sup>, Xiaohong Bai<sup>1</sup>, Peng Han<sup>1</sup>

<sup>1</sup> Department of Civil Engineering, Taiyuan University of Technology, Taiyuan, 030024, P. R. China

<sup>2</sup> State Key Laboratory of Hydraulic Engineering Simulation and Safety, Tianjin University, Tianjin, 300350, P. R. China

\*E-mail: [xieruizhen0094@link.tyut.edu.cn](mailto:xieruizhen0094@link.tyut.edu.cn), [liurun@tju.edu.cn](mailto:liurun@tju.edu.cn)

Received: 25 October 2016 / Accepted: 3 June 2017 / Published: 12 July 2017

As a common pipeline material, X70 steel has been extensively used in China (West-East Gas Pipeline Project), México and other countries. The macro-/micromorphology and surface composition of X70 steel in sand soil at exposure time of 35 d have been characterized using Canon 6D SLR cameras, SEM and EDS. To further study the effect of the heavy metal Zn ( II ) on the corrosion performance of X70 steel in sand soil, electrochemical corrosion tests (exposure times of 7 d and 35 d), polarization curves and EIS measurements have been conducted utilizing an electrochemical workstation. Additionally, six sand soil samples with various contents of Zn ( II ) were prefabricated. The results demonstrated that the addition of Zn ( II ) in sand soil clearly accelerated the corrosion process and affected the corrosion performance of X70 steel in sand soil. In non-contaminated sand soil, the corrosion products of X70 steel were mainly composed of Fe<sub>2</sub>O<sub>3</sub> and FeOOH etc... whereas the inner and outer layer iron-containing compounds constituted the corrosion products in Zn ( II )-contaminated sand soil. Moreover, the addition of Zn ( II ) in sand soil increased the degree of coverage and diversification of the corrosion products. The corrosion behaviour of X70 steel in non/low-contaminated sand soil ( $C_{\text{zinc (II)}} \leq 0.034\%$ ) exhibited localized corrosion, whereas in high-contaminated sand soil ( $C_{\text{zinc (II)}} = 0.068\% - 0.680\%$ ), uneven general corrosion was confirmed. Furthermore, in contaminated sand soil, the corrosion degree of X70 was the most severe at a Zn ( II ) content of 0.034%. A high content of Zn ( II ) (0.034%) accelerated the corrosion process. In addition, the Warburg impedance was observed in the EIS data of X70 steel in sand soil at exposure time of 35 d, and the reaction control step of the electrode reaction changed from activation control to diffusion control for X70 steel in Zn ( II )-contaminated sand soil.

**Keywords:** X70 steel; sand soil; Zn ( II ); corrosion performance; EIS

## 1. INTRODUCTION

X70 steel (American steel grade) is highly resistant to soil corrosion and has been used in China (West-East Gas Pipeline Project), México and other countries [1]. The transport of oil and natural gas mainly relies on a long-distance pipeline in China, which has been continuously developed [2-4]. However, the buried pipeline steel, which is in contact with different soil media, will inevitably corrode to various degrees due to soil moisture erosion, molten salt, oxygen and microorganisms. Local corrosion perforation leads to oil and gas leakage, interruption of transport, environmental pollution and serious economic losses and casualties [5, 6]. Additionally, there are an increasing number of underground pipes, casing pipes, storage tanks and other underground facilities [7]. Moreover, heavy-metal pollution, which is caused by an increasing number of fertilizer and pesticide applications and the discharge of industrial waste, negatively affects human health and environmental protection and has become increasingly serious [8, 9]. Zn, a major-pollutional heavy metal element in soil, not only decreases the engineering properties of soil (compressibility, shear strength, etc.) but also affects both the soil resistivity and corrosion [10-12]. Hence, the studies of the causes of pipeline corrosion and timely and effective measures for corrosion protection are important.

Resistivity, moisture content, pH, soluble salt content and temperature are the main factors that affect soil corrosion [13]. Physical and chemical property measurements, electrochemical tests, data processing and corrosion product analyses are four current types of research methods used to investigate the soil corrosion of metal materials [14-18]. Many researchers have contributed to rapid and accurate measurements of the corrosion rate of X70 steel in soil media and acquired the following results. In soils from five regions in Inner Mongolia, there are significant differences amongst the corresponding corrosion rates of X70 steel that have been buried underground for two years, and the corrosion rate ( $8.3 \text{ g/dm}^2 \cdot \text{a}$ ) in the Bameng region is the highest. Furthermore, all the corrosion rates of X70 steel that were buried underground for two years are lower than those buried for one year [19]. In a NACE solution with a  $\text{CO}_2$  partial pressure of 2 MPa, the corrosion rate (uniform corrosion) increased with temperature. Additionally, pitting corrosion was predominant at  $120 \text{ }^\circ\text{C}$  and was more evident under the action of  $\text{Cl}^-$  [20]. During a simulation of the corrosion environment of wet natural gas in oil and gas fields in a high-temperature and high-pressure condensation kettle, an increase in the moisture temperature increased the corrosion of X70 steel at a wall temperature of  $5 \text{ }^\circ\text{C}$ . However, an increase in the wall temperature slightly decreased the corrosion rate of X70 steel at temperatures of  $25 \text{ }^\circ\text{C}$  and  $45 \text{ }^\circ\text{C}$ . In addition, the corrosion morphology from  $25 \text{ }^\circ\text{C} \sim 45 \text{ }^\circ\text{C}$  exhibited comprehensive corrosion [21]. In a soil simulation solution from Qingdao, the X70 corrosion rate linearly increased with an increase in stray current density, and there was a difference between the DC and AC stray currents in the corrosion mechanism and pattern. Using an AC stray current, the corrosion amount was smaller (but more concentrated), and local corrosion was likely induced. In addition, the mixing of the DC stray current with the AC current substantially increased the metal corrosion rate [22].

There are many studies regarding the electrochemical behaviour of X70 in a soil simulation solution. In a near-neutral soil simulation solution (NS4), the existence of  $\text{CO}_2$  significantly increased the corrosion of X70 steel. The cathodic process included the reduction of  $\text{H}^+$ ,  $\text{H}_2\text{O}$ ,  $\text{H}_2\text{CO}_3$  and  $\text{HCO}_3^-$ , with the reduction of  $\text{H}_2\text{CO}_3$  and  $\text{HCO}_3^-$  predominating [23]. In an alkaline-simulated soil

solution for west Inner Mongolia (Baotou), the addition of a rare earth metal (cerium) in X70 steel increased the corrosion potential of the metal but inhibited uniform corrosion [24]. In a soil simulation solution that contained  $CO_2$  from Korla, China, the reaction between  $CO_2$  and a  $FeCO_3$  corrosion film formed a soluble Fe complex and accelerated the corrosion of X70 steel. Furthermore, a combination of hydrogen embrittlement and anodic dissolution led to stress corrosion cracking (SCC), and the effect of hydrogen embrittlement increased with an increase in  $CO_2$  partial pressure [25]. In a strong alkaline-simulated solution from a typical soil in Western China, X70 steel was more sensitive to  $SO_4^{2-}$  and  $Cl^-$ . Specifically, an increase in  $Cl^-$  concentration increased the corrosion current density of X70 steel and simultaneously intensified the pitting and overall corrosion. Furthermore, the adsorption of a small amount of  $SO_4^{2-}$  on the metal surface increased the pitting tendency, whereas the extensive coverage of  $SO_4^{2-}$  hindered the impact of  $Cl^-$  [26]. In addition, in saline soil with two humidities near Qinghai Salt Lake, the corrosion rate of X70 steel first increased and then decreased with an increase in humidity. The maximum value was acquired at a humidity of 15%~20%. However, the corrosion rate increased with an increase in soil salt content [27]. In contaminated soil from Shenyang, the inoculation of sulphate-reducing bacteria (SRB) increased the corrosion current of X70 steel by 1~2 orders of magnitude, and pitting appeared on the surface [28]. In 3.5 wt. % NaCl-simulated sandy soil, the corrosion of X70 steel was controlled by both cathodic diffusion and oxygen reduction, and the charge transfer resistance increased with particle size. Furthermore, the cathodic branch of the polarization curve for X70 steel positively shifted with increasing particle size, and the cathodic oxygen reduction process was also accelerated [29, 30]. There are also several studies regarding the electrochemical properties of X70 steel in other solution media, such as  $Na_2SO_4$  aqueous solution, laminar flow cooling water, a simulated solution of pipe crude oil, protic ionic liquids (PILs) and oilfield-produced water [31-35].

Overall, investigations regarding the corrosion of X70 steel were mainly focused on it in solutions and more concentrated in polarization. And relatively less focused on the corrosion evaluation of X70 steel in sand soil, heavy metal influences and a theoretical basis for the corrosion behaviour of X70 steel in sand soil. In this paper, a complete theoretical system for the corrosion behaviour of X70 steel in Zn (II)-contaminated sand soil was established, and the effect of Zn (II) on the corrosion performance of X70 in contaminated sand soil for 7 d and 35 d was also studied by methods based on electrochemical tests (polarization, impedance).

## 2. EXPERIMENTAL PROCEDURE

### 2.1 Experimental materials and pretreatment

X70 steel was selected for these experiments, and the components are shown in Table 1. The X70 steel plate was wire-cut into square test samples with dimensions of 15×15×2 mm. The working surfaces of the samples were then ground to a smooth finish using 320-800# sandpaper and subsequently polished to a bright appearance with no scratches utilizing 1000-2000# sandpaper when submerged in water. To avoid corrosion, the samples were immediately cleaned with alcohol, dried,

bagged and set aside after polishing. One end of a copper wire was fixed to the non-working surface of the sample by tin foil. In addition to the centre 1 cm<sup>2</sup> work areas, the other areas were sealed with AB glue. The soil sample cell had dimensions of 70.7×70.7×70.7 mm, and the two opposite faces were fixed with thin copper sheets of 70.7×70.7×0.2 mm to test the electrical resistivity ( $\rho_s$ ) of the soil samples.

**Table 1.** Chemical composition of X70 steel (wt. %)

C	Cr	Si	Mn	P	Ni	Mo	Cu	Co	V	S	Fe
0.065	0.021	0.201	1.906	0.012	0.021	0.234	0.012	0.013	0.011	<0.0005	Bal.

To comprehensively reveal the influence of Zn (II) in sand soil on the corrosion behaviour of X70 steel, six types of sand soils with various mass fractions of Zn (II) (0.000%, 0.034%, 0.068%, 0.170%, 0.340% and 0.680%) were chosen as the samples according to the actual situation.

**Table 2.** Mix proportion of sand contaminated by zinc (II)

C <sub>zinc (II)</sub> (%)	m <sub>sand</sub> (g)	Zn(NO <sub>3</sub> ) <sub>2</sub> •6H <sub>2</sub> O (g)	m <sub>w</sub> (g)	$\rho_s$ ( $\Omega\cdot m$ )
0.000	500	0.00	75.00	271.64
0.034	500	0.79	74.71	15.05
0.068	500	1.58	74.43	7.92
0.170	500	3.95	73.56	3.80
0.340	500	7.90	72.13	2.06
0.680	500	15.80	69.25	1.29

The composition and resistivity of different test soils were listed in Table 2. The resistivity of the soil samples was tested by digital AC bridge, model TH2828A (Tonghui, Changzhou of China). In this work, considering both the reduction in the electrochemical measurement precision with low water content and gap between the simulated soil corrosion with high water content and actual soil corrosion, a water content of 15% was selected as the parametric value. Using this value, the crystal water in the drug was also calculated [27]. When configuring the soil samples, a specific quantity of Zn(NO<sub>3</sub>)<sub>2</sub> solution (thoroughly dissolved) was sufficiently mixed with a specific amount of standard soil. Then, the samples were placed in a sealed bag for 24 h and subsequently removed into a labelled soil sample cell for the next tests. Furthermore, the compact degree of the soil samples, which was controlled by the soil height, was identical to avoid an error caused by a difference in the void ratio. To avoid other irrelevant factors that may influence this experiment (such as chloride ions and microorganisms, etc.), pure quartz sand (CHINA ISO STANDARD SAND CO., LTD.) was applied.

## 2.2 Test and characterization

The electrochemical tests were conducted on X70 steel samples with a work area of 1 cm<sup>2</sup> after they were embedded in prepared sand soil contaminated by zinc (II) for 7 d and 35 d using a CS350 electrochemical workstation (Wuhan Corrtest Instrument Co., Ltd). In addition, the steel samples were embedded at the same position in the soil, and soil sample cells were covered with plastic wrap to prevent the evaporation of moisture. Next, the soil sample cells were placed in a JK-VO-6020 thermo tank. The tests were performed at a temperature of 20±1 °C and a humidity of 45±2% in a three-electrode test system, which included an X70 steel working electrode, a saturated calomel reference electrode (SCE) and a platinum auxiliary electrode. The polarization curves were tested at a scanning speed of 0.5 mV/s and a scanning range relative to a corrosion potential of ±300 mV. Electrochemical impedance spectroscopy (EIS) was conducted at 10<sup>-2</sup>~10<sup>5</sup> Hz and a sinusoidal AC excitation signal amplitude of 5 mV. The micro-/macro-corrosion morphologies (before and after rust cleaning) of X70 steel embedded in soil samples for 35 d were acquired using scanning electron microscopy (SEM, Hitachi-TM 3000) and Canon 6D SLR cameras, respectively. The corrosion products were further tested utilizing energy dispersive spectrometry (EDS) on a Bruker Model QUANTAX combined spectrum analyser TM-3000.

## 3. RESULTS AND DISCUSSION

Clearly, the addition of zinc (II) decreased the resistivity of the soil samples. Soil resistivity, which reflects the conductivity of soil, is a comprehensive and extensively studied factor in soil corrosion research. In general, smaller soil resistivity exhibits greater soil corrosion. However, these properties do not have a linear relationship because the water and salt content in soil determines the value of soil resistivity to a certain extent. Additionally, the water and salt contents are significantly different in various soils. Hence, an evaluation that is based on a simple resistivity index often leads to misjudgements [18].

### 3.1 Macro-corrosion morphology

The macro-corrosion morphologies of X70 embedded in sand soil contaminated by various zinc (II) fractions for 35 d are shown in Figures 1 and 2 (before and after rust cleaning). Figure 1 shows that various degrees of corrosion occurred for the six group samples, and the corrosion increased with an increase in zinc (II) in sand soil. Corrosion products were formed on a large number of X70 steels and were difficult to remove by mechanical methods. The corrosion products directly formed on the specimens are hard substances and presented significant variations in colour from black and brown to red-brown and white. Moreover, there was no significant corrosion pitting on X70 steel in sand soil with zinc (II) contamination before rust cleaning, which was different with that in copper (II)-contaminated soil that was previously studied [37]. This difference may be caused by a difference in the standard electrode potentials of zinc (II) and copper (II) relative to Fe. Additionally, white corrosion products on X70 steel increased with increasing zinc (II) contamination in sand soil;

however, at a zinc (II) content of 0.680%, the white corrosion products with a minor amount of red-brown covered most regions. In contrast, for X70 steel in sand soil without contamination, the highest corrosion pitting was in the middle of the specimen, whereas limited corrosion pitting and areas that were not covered by corrosion products occurred at the specimen edges. This behaviour is typical of localized corrosion.

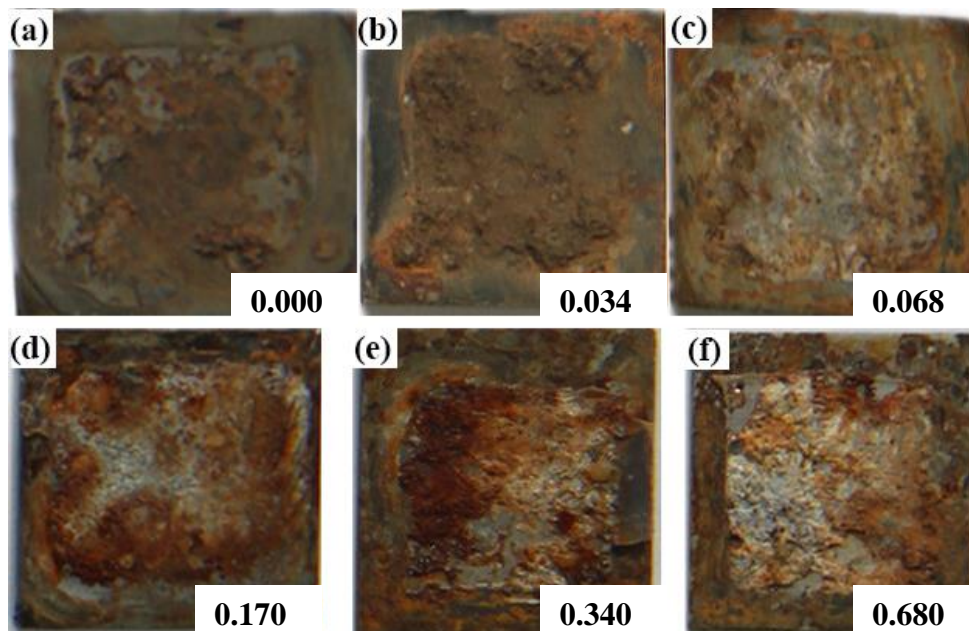


**Figure 1.** Macro corrosion morphology of X70 steel in sand soil with different content of zinc (II) for 35 d (Before rust cleaning): (a) 0.000%, (b) 0.034%, (c) 0.068%, (d) 0.170%, (e) 0.340%, (f) 0.680%.

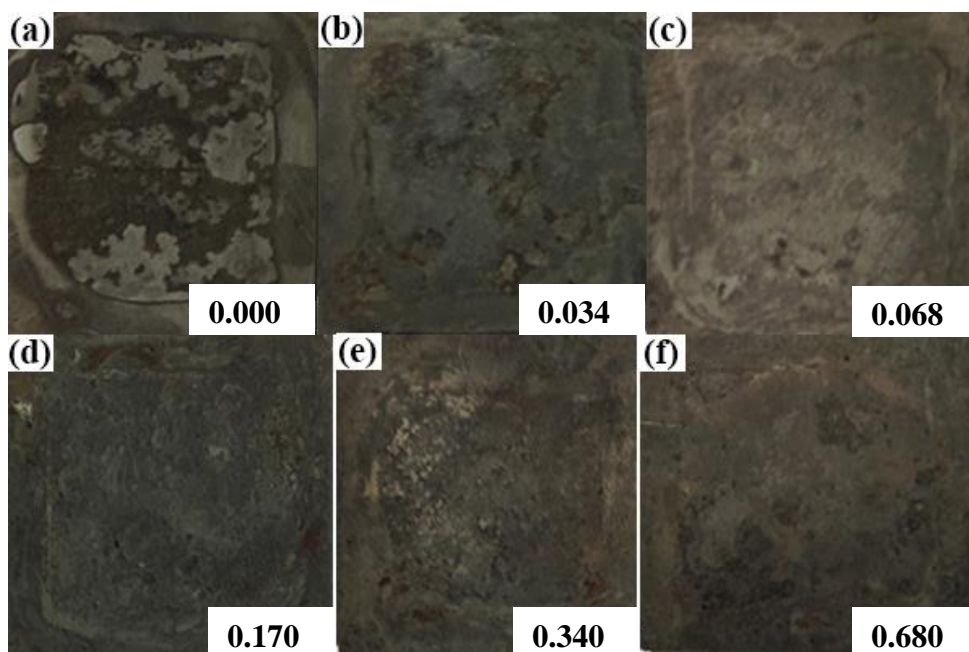


**Figure 2.** Macro corrosion morphology of X70 steel in sand soil with different contents of zinc (II) for 35d (After rust cleaning): (a) 0.000%, (b) 0.034%, (c) 0.068%, (d) 0.170%, (e) 0.340%, (f) 0.680%.

The macro-corrosion morphologies (Figure 2) of X70 steel in sand soil for 35 d (after rust cleaning) showed that in zinc (II)-contaminated sand soil, the corrosion of X70 steel was most severe at a content of 0.034%. There were several deep and shallow corrosion pits that were felt by touching the steel specimens, which is different from that of X70 steel in sand soil without contamination. At zinc (II) contents of 0.068%-0.680%, the corrosion morphology and degree of X70 were similar. The corrosion pits were fewer in number and shallow, and the corrosion degree was uniform over of the entire surface. The specimens presented a dim metallic lustre and were smooth. Generally, both the corrosion of X70 steel in sand soil without zinc (II) contamination and with a low content of zinc (II) (0.034%) are both considered localized corrosion. X70 steel in sand soil with a high content of zinc (II) (0.068%-0.680%) is considered uneven general corrosion. Nevertheless, the corrosion of X70 steel in copper (II)-contaminated soil belongs to a typical localized corrosion process [37].

In sand soil both with a low content of zinc (II) (0.034%) and without zinc (II) contamination, the corrosion process is mainly controlled by oxygen depolarization on the cathode. When an uneven liquid film forms on the electrode surface due to the uneven arrangement of sand particles, a difference in oxygen concentration formed on the surface of electrode, and oxygen concentration cell occurred. The electrode potential of the anoxic area was lower than that of the oxygen-rich area. Thus, the anoxic area becomes the anode, and the metal was corroded [38]. In the anoxic area, more  $\text{Fe}^{2+}$  gathered in the liquid, and the hydrolysis of cations decreased the pH. In oxygen-rich areas, the oxygen discharge increased the pH, and an autocatalytic effect of the corrosion process was initiated. Thus, the corrosion degree in the anoxic zone became more severe, and deep corrosion pits were formed, which further led to the accumulation of  $\text{Fe}^{2+}$  and the formation of localized corrosion. On X70 steel in sand soil contaminated by a high content of zinc (II) (0.068%-0.680%), the coverage of Zn-containing compounds changed the corrosion of X70 steel to a uniform corrosion process.

### 3.2 Microscopic corrosion morphology

The X70 steel samples were embedded in sand soil contaminated by various contents of Zn (II) for 35 d, and then the sand particles on the surface were cleaned. Next, low- and high-magnification ( $\times 30 \sim \times 1000$ ) images of the microscopic corrosion morphology of the X70 samples (prior to rust cleaning) were acquired, as shown in Figure 3. In the samples without contamination (Figures 3a and b), there was a relatively thin corrosion product layer (light grey), a thick corrosion product layer (dark grey), deep corrosion pits (black) and a small amount of pitted (white) local areas on the surface of the X70 samples. Furthermore, needle-like and scaly corrosion products were present in the corrosion pits, and several micro-cracks were present on the product layer, which can be explained by Stress Corrosion Cracking (SCC) due to anodic dissolution and hydrogen-induced cracking [39-41]. The addition of zinc (II) to sand soil increased the diversification and degree of coverage of the corrosion products on the X70 samples, as shown in Figures 3c-3f. The corrosion product layers were thicker and presented an obvious hierarchical structure. In contrast, a bud-like corrosion product (shown Figure 3e) is a typical morphology of iron-containing compounds and were presented in many areas. A

more free and sheet-tufted material (shown in Figure 3f) was the corrosion product (Zn compound) on the outermost layer.

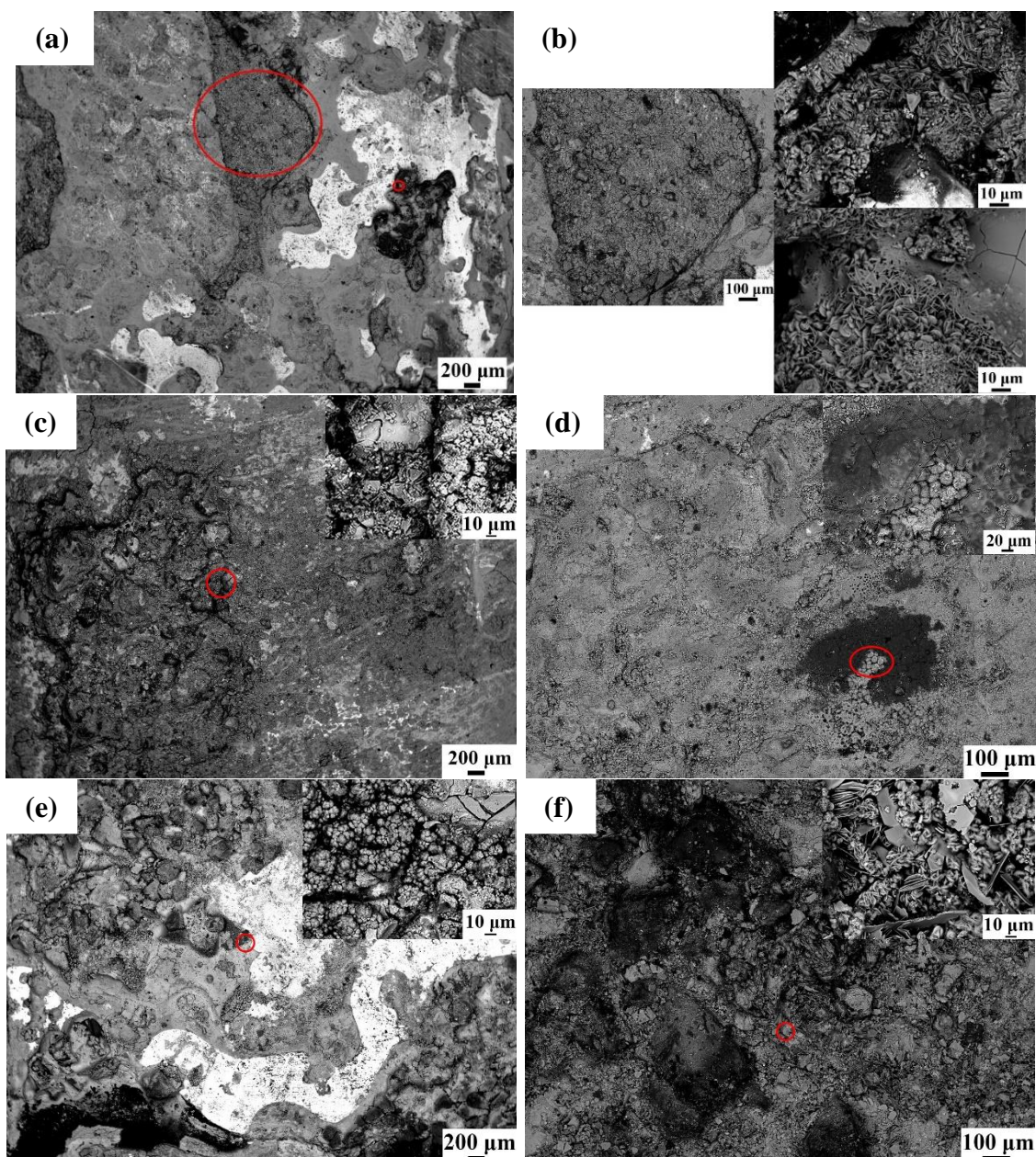


**Figure 3.** Micro morphology of X70 steel in sand soil with different contents of zinc (II) for 35 d (Before cleaning rust): ( a, b) 0.000%, (c) 0.034%, (d) 0.068%, (e) 0.340%, (f) 0.680%.

Figure 4 shows SEM micro-corrosion morphologies of the X70 samples after rust cleaning. Clearly, there are several differences between corrosion morphologies of the X70 samples in sand soil with and without zinc (II) contaminants. When the content of zinc (II) was 0.034%, deep-shallow corrosion pits substantially covered the entire surface, and the surface presented a delamination. When the content of zinc (II) ranged from 0.068%-0.680%, the corrosion morphologies were similar, and the area and depth of corrosion pits were reduced compared with that observed at 0.034%. In addition, SEM corrosion morphologies at high-magnification demonstrated that local area pitting is more severe.

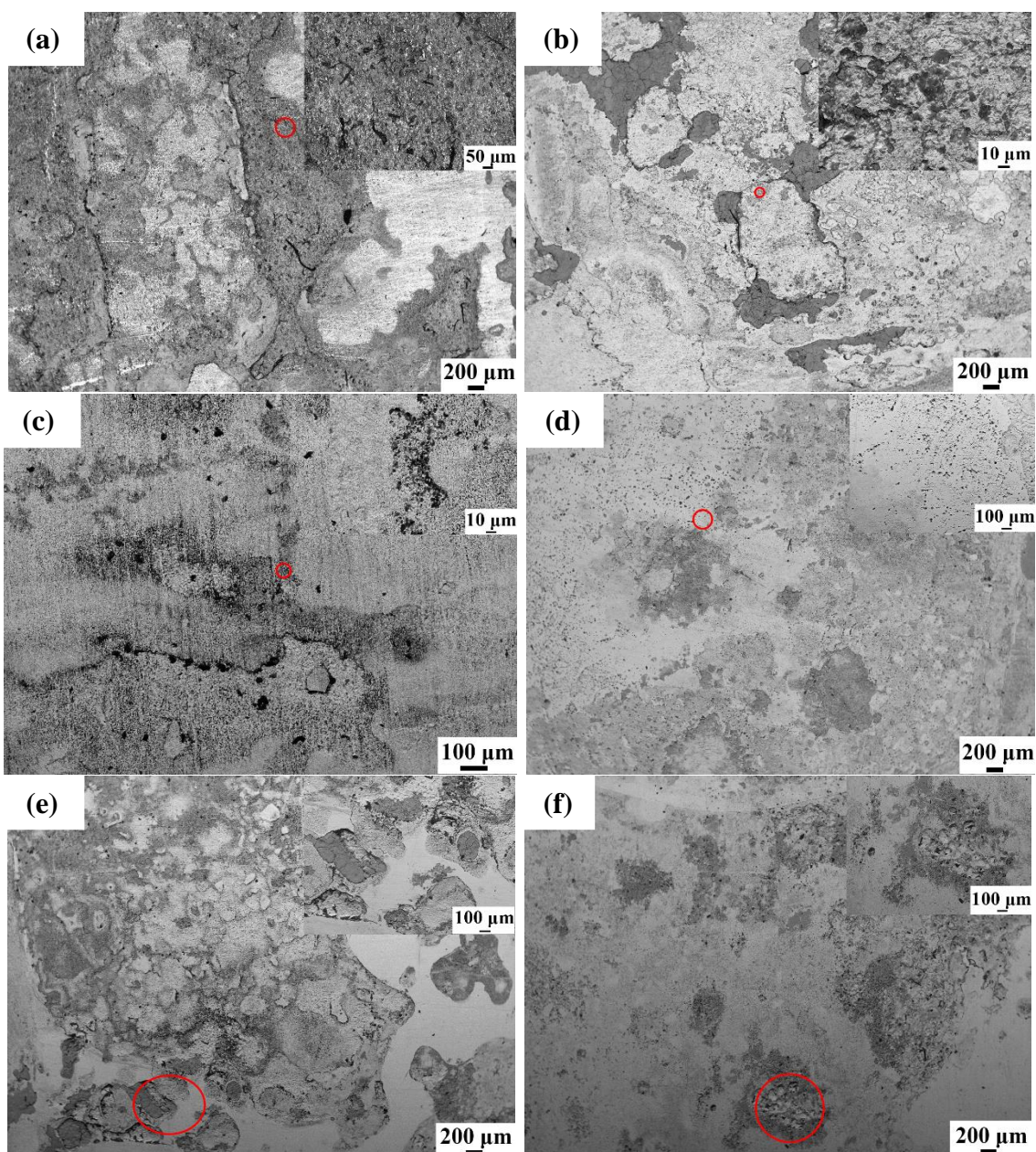


**Figure 4.** Micro morphology of X70 steel in sand soil with different contents of zinc (II) for 35 d (After cleaning rust): (a) 0.000%, (b) 0.034%, (c) 0.068%, (d) 0.170%, (e) 0.340%, (e) 0.680%

### 3.3. Results of EDS

Figures 5 and 6 show the EDS test results for the distributions and mass percentages of the main elements, respectively, of a typical X70 steel surface after 35 d in sand soil contaminated by different zinc (II) fractions (0.000%, 0.034%, 0.068%, 0.170%, 0.680%). For X70 steel in the sand soil without zinc (II) contamination, Fe was evenly distributed on the surface, and O was concentrated in the darker areas. Moreover, there is basically no O in the white area, as shown in Figure 5. On a typical surface of X70 steel in sand soil with 0.170% zinc (II) contamination, more Zn appeared in the corrosion products, and a shift phenomenon, which always alters or replaces each element, occurred in the distribution of Fe and Zn.

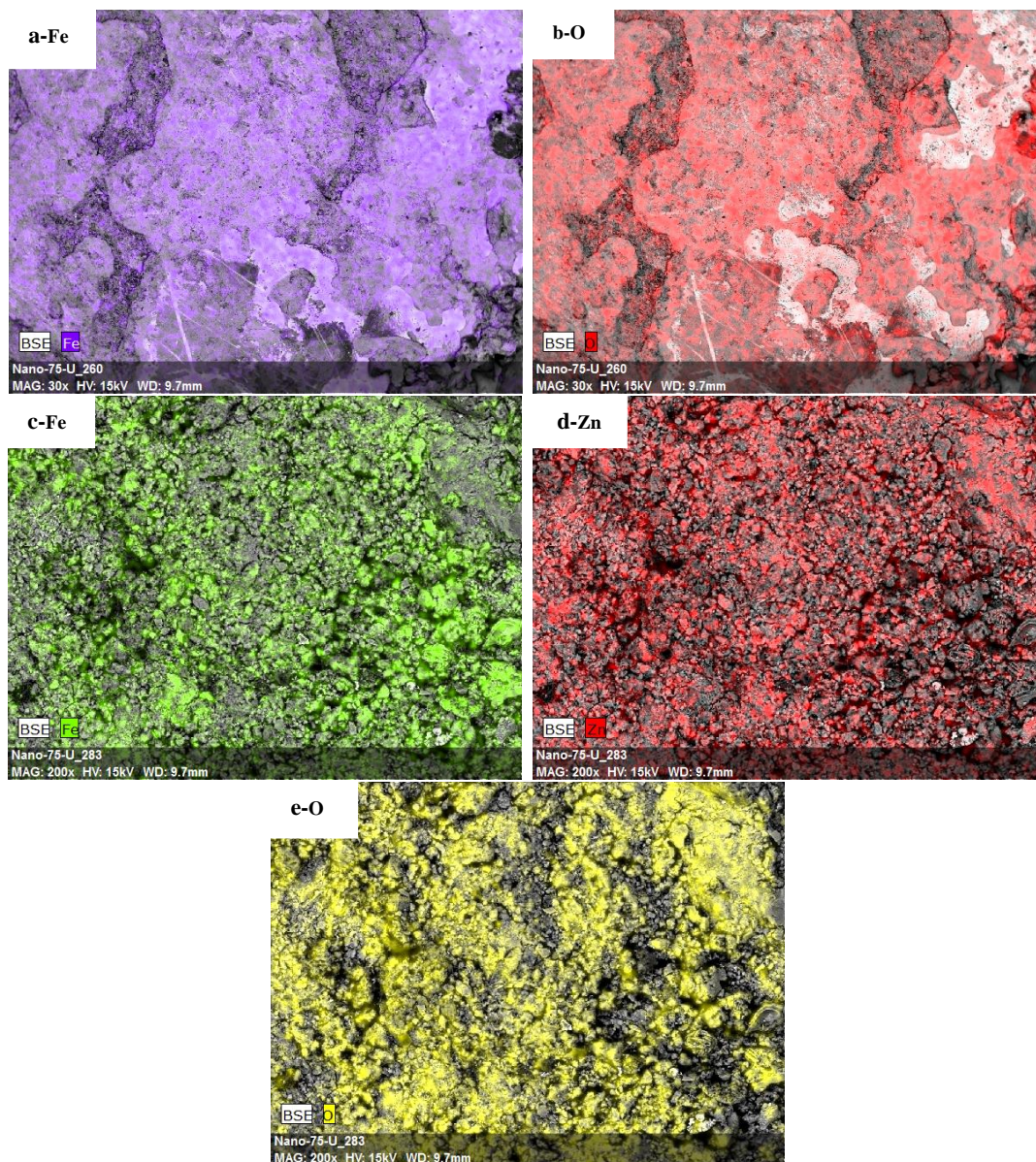


**Figure 5.** Surface element distribution of X70 in uncontaminated sand soil (a, b) and 0.170%-zinc (II) contaminated sand soil (c, d, e).

The mass percentages of the main elements for three typical corrosion areas (white, light grey and dark grey in Figures 6 a, b and c, respectively) on the X70 steel surface in uncontaminated sand were determined. The mass percentage for Fe was more than 80% in the white area, and the quality percentages of Fe and O (approximately 65% and 30%, respectively) were similar in light and dark grey areas. Specifically, fewer corrosion products were generated in the white area, whereas more corrosion products were produced in the light and dark grey areas, which were mainly composed of Fe and O elements and may be associated with  $Fe_2O_3$  and FeOOH, etc. In contrast, in the corrosion products of X70 steel in sand soil contaminated by 0.170% and 0.680% zinc (II), the percentage of Zn increased to 43.5% and 53.2%, respectively, whereas Fe decreased to 19.1% and 2.6%, respectively. These data indicated that a large number of  $Zn^{2+}$  in sand media were involved in the formation of

corrosion products from the outside to the inside, which was accumulated through zinc-containing compounds that were formed by the combination of  $Zn^{2+}$  and  $OH^-$  from the electrode surface to the outside layer-by-layer. However, the combination of  $Fe^{2+}$  and  $OH^-$  was from the electrode surface to the inner layers, and the iron-containing compound was accumulated from the electrode surface to the inside, layer-by-layer. Thus, hierarchical corrosion products were formed on the surface of the electrode, which consisted of the outer layer of zinc-containing compounds and the inner layer of iron-containing compounds. This also explains the phenomenon that there was more Zn than Fe in the corrosion products. Figure 6 also indicates that sheet-tufted material was a typical Zn-compound, which is consist with the micro-morphology results (3.2).

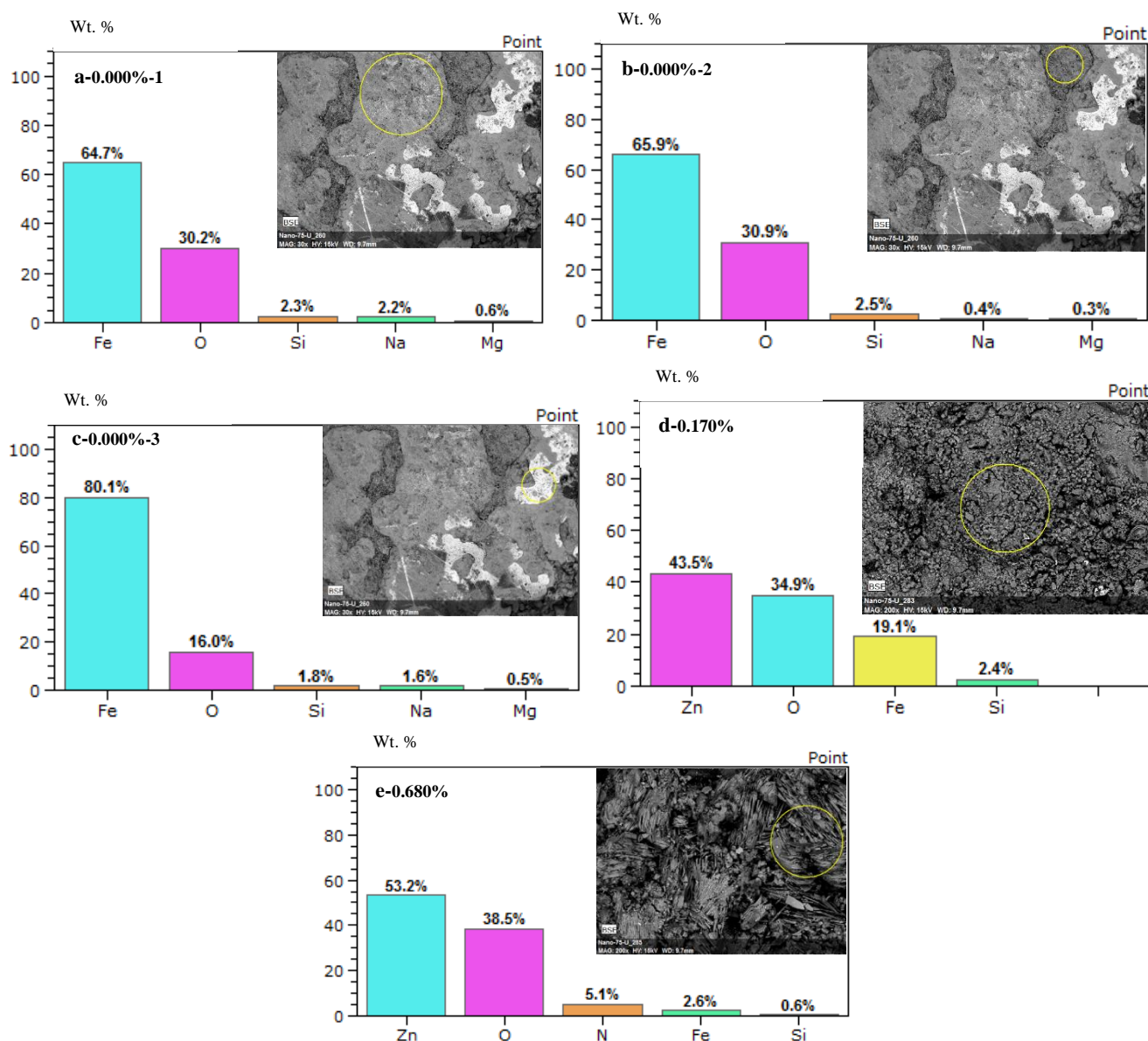


**Figure 6.** Element mass percent of the X70 steel surface in uncontaminated sand soil (a, b, c) and typical zinc (II) contaminated sand soil (d-0.170%, e-0.680%)

### 3.4 Polarization curve analysis

#### 3.4.1 Polarization curve of X70 steel at exposure time of 7 d

Polarization curves and fitting results of X70 steel embedded in sand soil and contaminated by various fractions of zinc (II) are shown in Figure 7 and Table 3, respectively. Overall, as the zinc (II) contamination increased, the polarization curves shifted upward, and the corrosion potential increased from -783 mV to -608 mV. Additionally, the corrosion of X70 steel was more controlled by the dissolved oxygen diffusion control of cathodic depolarization than the diffusion control of the anodic reaction [33-35]. This situation can be explained as follows. In the X70/sand system, a pair of conjugate electrochemical reactions (anodic dissolution of iron and reduction of the cathodic depolarizer) occurred on the surface of the X70 steel electrode due to the existence of water and dissolved oxygen in the liquid phase of sand soil. Then, the reactions proceeded irreversibly in the direction of electrode corrosion before achieving a steady-state in the system. In sand soil without zinc (II) contamination,  $Fe^{2+}$  that was desorbed from the electrode surface directly combined with  $OH^-$  in the cathode region. Corrosion products, such as  $Fe(OH)_2$  and  $Fe_2O_3$ , were subsequently formed through a series of reactions. The addition of zinc (II) contamination in sand soil led to the existence of  $Zn^{2+}$  in the corrosion system and the formation of  $Zn(OH)_2$  in the cathode region. The attachment of zinc compounds to the electrode surface hindered both the diffusion of  $Fe^{2+}$  cations to the sand media and the diffusion of reducing species from sand to the steel surface. To some extent, the accumulation of  $Fe^{2+}$  on the electrode surface was consistent with energy spectrum analysis results (3.3). Thus, the corrosion potentials were increased. At zinc (II) contents of 0.170%, 0.340% and 0.680% in sand soil, inflection points appeared in the strong polarization region of the anode, and the anodic branch presented a steep and then gentle slope, which may be due to surface state changes. In addition, the end slopes of the three groups of the anodic branch were significantly smaller than those at low zinc (II) content.

Tafel linear fitting results of the polarization curves at a 100 mV~200 mV (up and down) open-circuit potential are shown in Table 3 [42]. It was concluded that the addition of Zn (II) contamination in sand soil accelerates the corrosion of X70 steel. At low content zinc (II) contamination, the corrosion current density of X70 steel increased rapidly with an increase in zinc (II) content. When concentration of zinc (II) contamination was 0.068%, the corrosion current density reached a maximum value of  $4.945 \mu A/cm^2$ , which was an increase of more than 4 times that ( $1.178 \mu A/cm^2$ ) in sand soil without contamination. When the content of zinc (II) contamination increased continuously to 0.170%, the corrosion current density of X70 steel sharply decreased to  $1.620 \mu A/cm^2$ . However, with a further increase of zinc (II) content in sand soil, the corrosion current density slightly increased again. According to the electrochemical evaluation standards, the addition of zinc (II) in sand soil strengthens the corrosion of X70 at exposure time of 7 d (slight corrosion (I)). However, the corrosion of X70 samples in all zinc(II)-contaminated soil samples generally exhibited slight corrosion (I) behaviour and only at individual contents of 0.068% and 0.680%, the corrosion achieved a medium corrosion (II) designation [42].

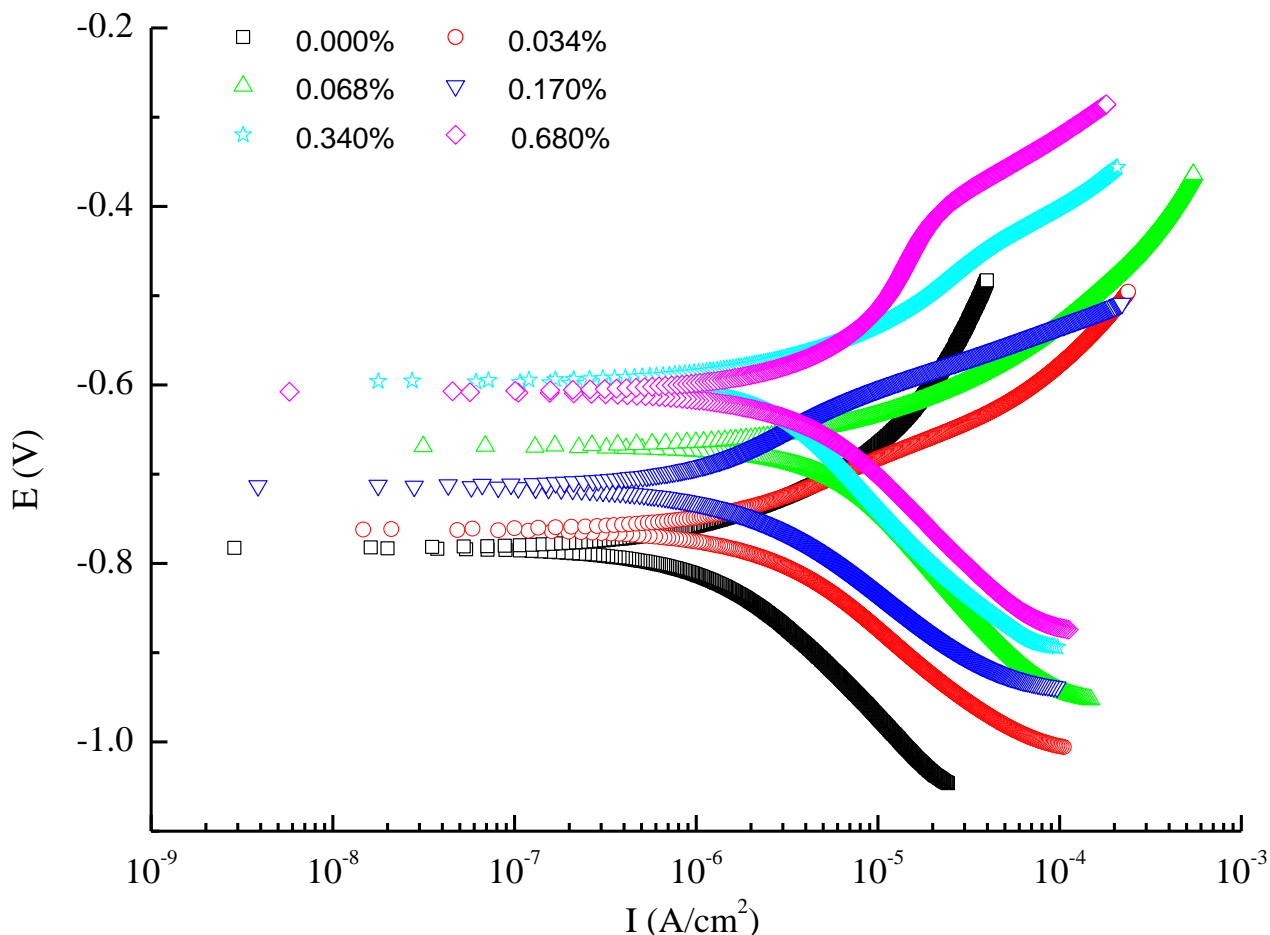


**Figure 7.** Polarization curves of X70 steel in contaminated sand with different zinc (II) content (exposure time of 7 d): 0.000%, 0.034%, 0.068%, 0.170%, 0.340% and 0.680%

Faraday's law indicates that there is an equivalent relationship between the amount of substance change for an electrode reaction and the amount of charge transfer [43]. The greater the corrosion current density, the greater the erosion effect of the medium on the material and vice versa. Generally, zinc (II) contamination in sand soil promotes the corrosion of X70 steel and corrosion rates are all enhanced to various degrees. The sharp decrease in corrosion rate with a zinc (II) content of 0.068%~0.170% indicated that the surface state of the electrode or the electrode reaction greatly changed. The possible reason is that the higher content of  $Zn^{2+}$  in sand soil led to the agglomeration of particles and appearance of larger pores [9]. Thus, the progress of hydrogen evolution reaction was promoted, and the corrosion rate of iron was increased by an increase in zinc (II) contamination in sand soil. However, when the content of zinc (II) was 0.170%, the adhesion of a large amount of reaction product particles on the electrode surface hindered the diffusion of substances and reduced the corrosion rate. When the contaminant content was above 0.170%, the secondary increase in corrosion current density could be attributed to the partial mechanical destruction of sand particles, a reaction of product particles, and the further advancement of the corrosion of X70 samples [29, 30].

**Table Error! No text of specified style in document..** Fitted results for polarization curves of X70 steel in sand contaminated by zinc ( II ) (exposure time of 7 d)

$C_{\text{zinc(II)}} (\%)$	$I_{\text{corr}}(\mu\text{A}/\text{cm}^2)$	$E_{\text{corr}} (\text{V})$
0.000	1.178	-0.783
0.034	2.096	-0.762
0.068	4.945	-0.669
0.170	1.620	-0.713
0.340	2.119	-0.596
0.680	3.362	-0.608

3.4.2 Polarization curve of X70 steel corroded at exposure time of 35 d

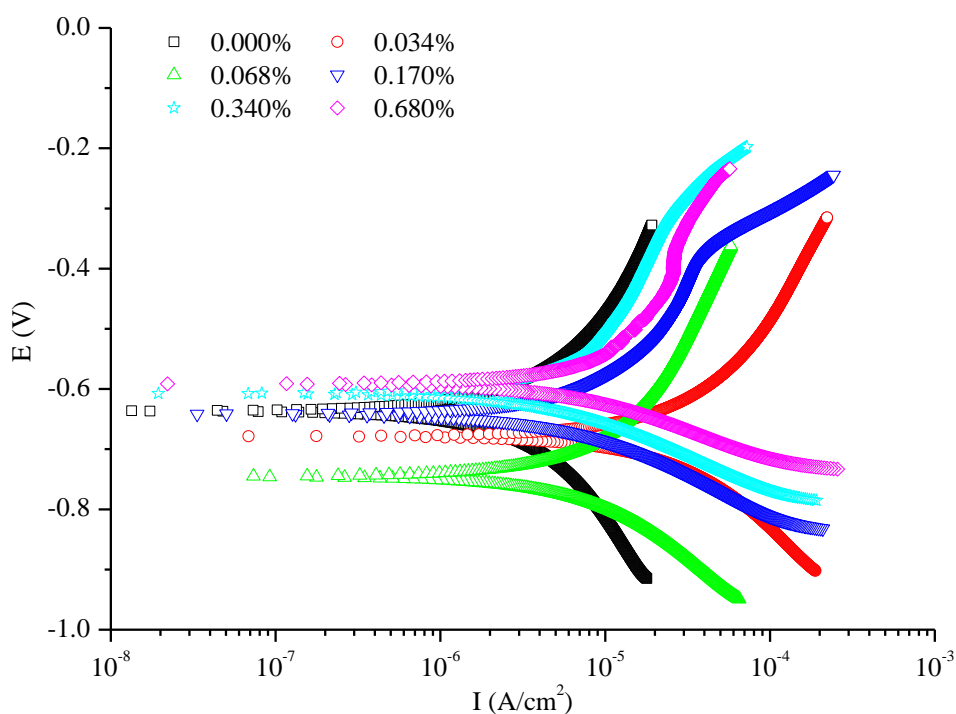


**Figure 8.** Polarization curves of X70 steel in contaminated sand with different zinc ( II ) content (exposure time of 35d): 0.000%, 0.034%, 0.068%, 0.170%, 0.340%, and 0.680%

Figure 8 shows polarization curves of X70 steel embedded in sand soil contaminated by various contents of zinc ( II ) for 35 d. In sand soil at a low zinc ( II ) content ( $\leq 0.068\%$ ), there was an obvious Tafel linear region in the polarization curve, whereas at a high zinc ( II ) content ( $\geq 0.068\%$ ), an inflection point appeared in the anode branches, and a new plateau appeared above it, which also

exhibited the change of electrode surface state in the strong polarization region of the anode. Tafel fitting results for the polarization curves are shown in Table 4. In sand soil with low zinc (II) contents of 0.000%, 0.034%, 0.068% for 35 d, the corrosion potential of X70 steel negatively shifted with an increase in zinc (II) content (from -636 mV to -746 mV). When the zinc (II) content further increased, the corrosion potential presented a significantly positive shift, which was different from that for 7 d.

The maximum value of the corrosion current density of X70 steel ( $21.376 \mu\text{A}/\text{cm}^2$ ) was acquired at a zinc (II) content of 0.034%. The density value decreased and then attained a steady state value with a further increase in zinc (II) in sand soil, and the corrosion rate of the X70 samples also correspondingly changed. Similarly, according to the standards, zinc (II) contamination in sand soil deteriorated the corrosion of X70 on the basis of moderate corrosion (II) behaviour at exposure time of 35 d. However, in all zinc (II)-contaminated soils, the corrosion of X70 samples generally belongs to the slight corrosion (I) category, whereas at an individual content of 0.034%, severe corrosion (IV) occurred to the X70 steel. In addition, the corrosion degree grade of all X70 samples generally decreased with an increase in exposure time (changing from slight corrosion (I) at exposure time of 7 d to moderate corrosion (II) at 35 d) [40]. According to solubility product principles,  $\text{OH}^-$  will preferentially react with  $\text{Fe}^{2+}$  when  $\text{Zn}^{2+}$  and  $\text{Fe}^{2+}$  are simultaneously present in the solution and  $\text{OH}^-$  will react with  $\text{Zn}^{2+}$  when the  $\text{Zn}^{2+}$  content is sufficiently high. As described above, the presence of zinc (II) had two roles: accelerating and inhibiting the corrosion of X70 steel. The presence of zinc (II) also accelerated the corrosion of X70 steel, and at high zinc (II) content, the corrosion accelerated more rapidly. When the zinc (II) content was low (0.034%), the pores in the sand layer were still small, the micro-battery was greater and the active area was larger [9]. Hence, the maximum value of the corrosion rate was attained. With an increase in zinc (II) contamination, the sand layer pores became larger, and the increase in corrosion products coverage on the electrode surface hindered the diffusion of the substance, thereby protecting the electrode from corrosion. A further increase of zinc (II) promoted the balance between the adsorption and desorption of the corrosion product layers. Thus, the corrosion rate was stable at high zinc (II) content.

**Table 4.** Fitting results of polarization curves for X70 steel in zinc (II) contaminated sand soil (exposure time of 35 d)

$C_{\text{zinc (II)}} (\%)$	$I_{\text{corr}} (\mu\text{A}/\text{cm}^2)$	$E_{\text{corr}} (\text{V})$
0.000	3.629	-0.637
0.034	21.38	-0.679
0.068	6.178	-0.746
0.170	5.171	-0.642
0.340	5.578	-0.608
0.680	5.005	-0.592

From Table 4, we also concluded that the addition of zinc (II) in sand soil promotes the corrosion of X70 steel. The corrosion current density of X70 steel in different sand soils for 35 d was higher than that in various sand soils for 7 d, and the protection of corrosion products decreased. This behaviour may relate to the continuous growth of the corrosion product layer that caused a continual rise in internal stress, which collapsed the cracks. Moreover, the substrate was re-exposed to the corrosive medium [34, 35]. Because of the larger pores in contaminated sand soil with higher zinc (II) content, the corrosion of X70 steel progressed faster, and the interface rapidly reached a steady state. Thus, the corrosion current density fluctuated at approximately  $5 \mu\text{A}/\text{cm}^2$  when the content of zinc (II) was above 0.068%.

### 3.5 EIS analysis

EIS sensitively shows the change at the interface of the metal/sand layer. In sand soil, a sand layer with large resistance and small capacitance is equivalent to an insulating layer that prevents or delays the permeation of electrolyte solution into the interface of the metal/sand layer [45, 46]. Thus, the sand layer acts like a protective layer of metal. At a certain exposure time, the electrolyte solution permeated the interface of the metal/sand layer and a corrosion microcell was formed. The corresponding EIS data exhibited two time constants [45, 46]. EIS in the high-frequency region is the response of the capacitance and resistance ( $C_s$ ,  $R_s$ ) for the sand layer near the metal, whereas EIS in a low-frequency region is the response of the double-layer capacitance at the interface ( $C_{dl}$ ), polarization resistance and corrosion reaction resistance ( $R_{ct}$ ) for the metal.

#### 3.5.1 EIS of X70 steel corroded at exposure time of 7 d

Figure 9 shows the EIS data of X70 steel in six types of sand soil with different contents of zinc (II) contamination after for 7 d. The results show that when the zinc contamination in sand soil increased, the EIS data changed from a two-capacitive arc to an incomplete capacitive arc (high frequency), a complete capacitive arc (mid-low frequency) and a small inductive arc (low frequency). The inductive arc may be caused by metal ions formed by the activation of the working electrode [33]. This indicates that the Zn contaminant in sand soil influenced the corrosion process and surface state of X70 steel and the electrochemical polarization. The concentration polarization simultaneously existed in the cathodic process of the metal electrode [35, 36]. Overall, the addition of zinc (II) in sand soil decreased the capacitive arcs. Furthermore, the minimum and maximum arcs in contaminated sand soil were successively acquired in sand soil with 0.068% and 0.170% zinc (II), respectively. In sand soil without zinc (II) contamination, the two complete and large capacitive arcs indicated that, in addition to the electrode potential ( $E$ ), there was another variable state during the surface process of the X70 steel electrode after being exposed for 7 d. In zinc (II)-contaminated sand soil, the impedance spectroscopy measurements presented capacitive arcs that are much smaller than those in sand soil without zinc (II), especially in the high-frequency region. This behaviour may be explained by a

change in properties of the sand layer (electrical resistivity ( $\rho_s$ ),  $C_s$  and  $R_s$ ) due to the permeation of the electrolyte solution into the sand soil.

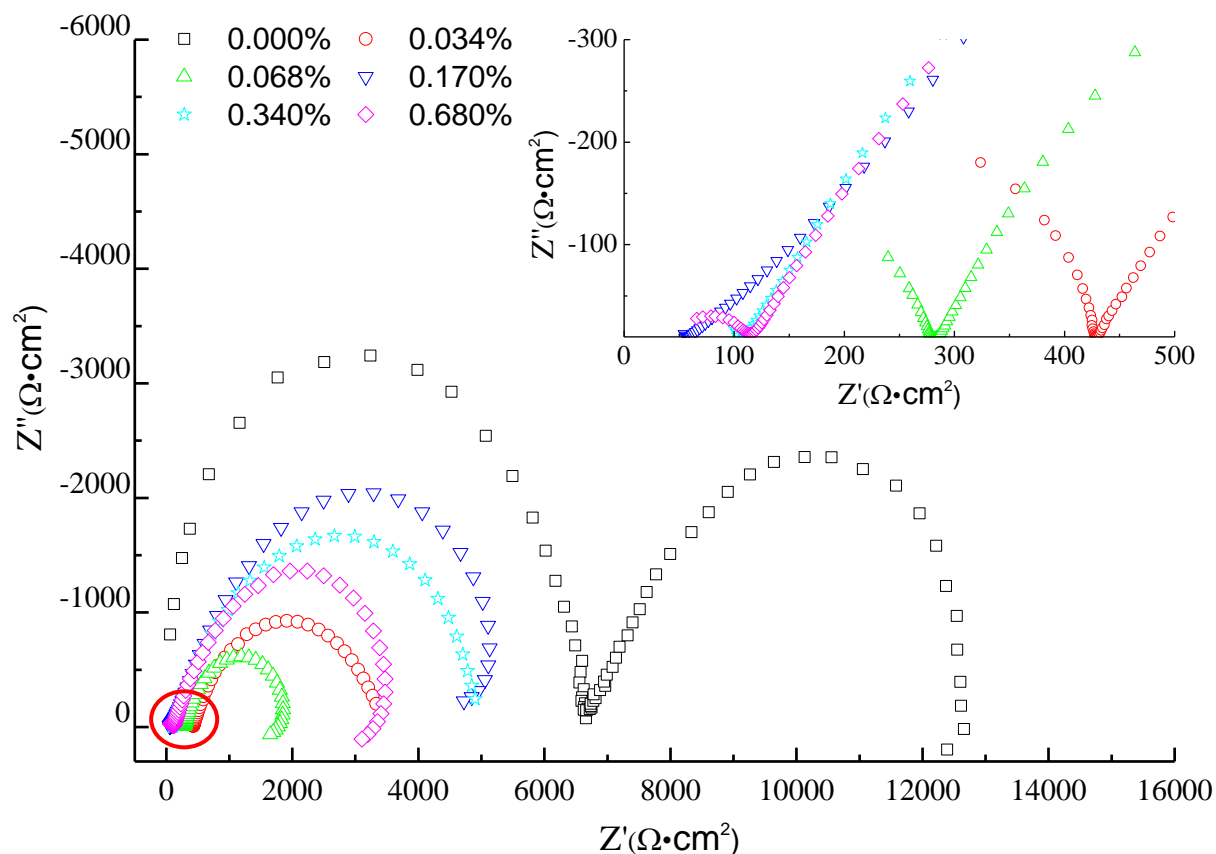


**Figure 9.** EIS of X70 steel in contaminated sand with different zinc (II) content (exposure time of 7d): 0.000%, 0.034%, 0.068%, 0.170%, 0.340%, 0.680%

To better analyse the change process of metal/sand layer system, EIS data of X70 in sand soil without and with a low content of zinc (II) (0.000%, 0.034% and 0.068%) were fitted by the equivalent circuit (Figure 10A). In this work, the EIS data were fitted through ZsimDemo software, and the results are shown in Figures 11(a), (b), (c) and Table 5. Alternatively, the EIS data of X70 in sand soil with a high content of zinc (II) (0.170%, 0.340% and 0.680%) were fitted by the equivalent circuit (Figure 10B), and the results are shown in Figure 11(d), (e) and (f), respectively, and Table 5. Amongst the components,  $R_l$  is the resistance of the electrolyte solution, which is too small to discuss;  $Q_s$  is the capacitance of the sand layer;  $R_s$  is the resistance of the sand layer;  $Q_{dl}$  is the capacitance of the double layer; and  $R_{ct}$  is the charge transfer resistance. The results show that the addition of Zn (II) contamination in sand soil accelerated the mass transfer process of the electrolyte, and so the EIS model of metal/sand changed from A to B [45, 46].

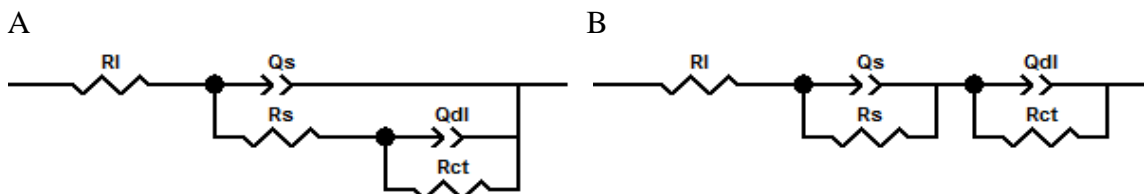


**Figure 10.** Equivalent circuit for low frequency region in EIS of X70 steel in zinc (II) contaminated sand (exposure time of 7d): A, 0.000%, 0.034%, 0.068%; B, 0.170%, 0.340%, 0.680%.

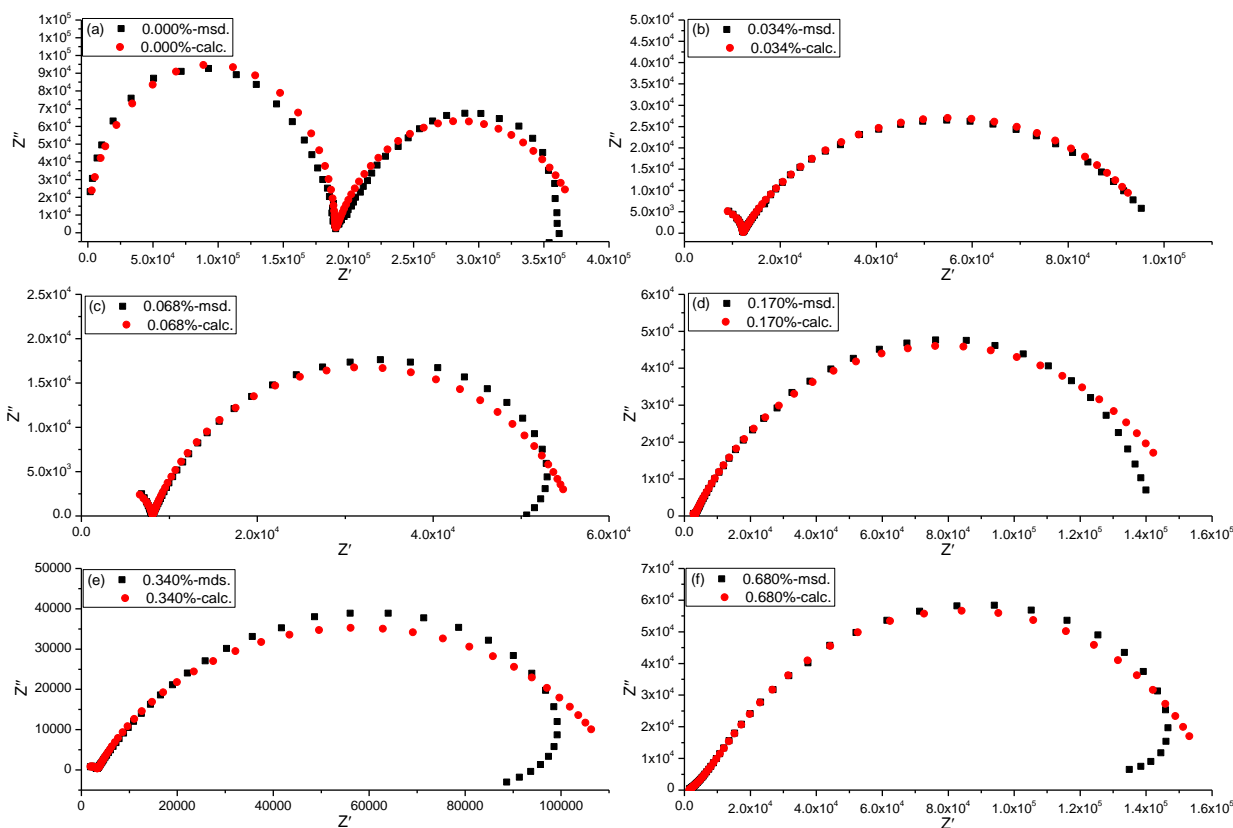


**Figure 11.** Fitted results for EIS of X70 steel in sand soil contaminated by zinc (II) (exposure time of 7d): (a) 0.000%, (b) 0.034%, (c) 0.068%, (d) 0.170%, (e) 0.340%, (f) 0.680%

Furthermore, the corrosion reaction of metals were also accelerated. In non/low-contaminated sand soil, the sand layer was a near-pure capacitance component ( $Q_s-n \approx 1$ ). With an increase in zinc (II) content,  $R_s$  decreased by 1~2 orders of magnitude, whereas  $C_s$  rapidly increased by several orders of magnitude. Moreover, countless tiny flat-plate capacitors formed the double layer of electrode surface, and  $Q_{dl-n}$  ( $\approx 0.7$ ) was generally smaller than that in solution ( $\approx 1$ ) [47]. Overall,  $R_{ct}$  also decreased and then reached a stable value with a magnitude of  $10^5$ . In low-contaminated sand soil, the decrease of  $R_{ct}$  was caused by the coverage of corrosion products. With a further increase of zinc (II), the coverage of the corrosion product on the metal surface hindered the transfer of charge. At higher fractions of zinc (II) contamination, the relatively stable  $R_{ct}$  may be related to the stabilization of active zones, corrosion product layer and sand soil particles on the steel.

**Table 5.** Fitted results of EIS for X70 steel in sand soil contaminated by zinc (II) (exposure time of 7d)

$C_{\text{zinc(II)}} (\%)$	$R_l (\Omega \cdot \text{cm}^2)$	$Q_s$		$R_s (\Omega \cdot \text{cm}^2)$	$Q_{dl}$		$R_{ct} (\Omega \cdot \text{cm}^2)$
		$Q_{s-Y_0} (\Omega^{-1} \cdot \text{cm}^{-2} \cdot \text{s}^{-1})$	$Q_{s-n}$		$Q_{dl-Y_0} (\Omega^{-1} \cdot \text{cm}^{-1})$	$Q_{dl-n}$	
0.000	$8.04 \times 10^{-2}$	$5.69 \times 10^{-11}$	1.00	$1.90 \times 10^5$	$4.58 \times 10^{-6}$	0.741	$1.91 \times 10^5$
0.034	$4.53 \times 10^{-7}$	$9.35 \times 10^{-11}$	0.97	$1.22 \times 10^4$	$6.96 \times 10^{-6}$	0.712	$8.63 \times 10^4$
0.068	$6.70 \times 10^{-3}$	$3.92 \times 10^{-10}$	0.87	$8.11 \times 10^3$	$6.02 \times 10^{-6}$	0.776	$4.80 \times 10^4$
0.170	$1.32 \times 10^{-2}$	$7.23 \times 10^{-10}$	0.86	$3.05 \times 10^3$	$5.73 \times 10^{-6}$	0.698	$1.51 \times 10^5$
0.340	$7.14 \times 10^2$	$3.24 \times 10^{-8}$	0.71	$2.69 \times 10^3$	$3.32 \times 10^{-6}$	0.735	$1.08 \times 10^5$
0.680	$1.38 \times 10^3$	$1.79 \times 10^{-5}$	0.42	$2.65 \times 10^4$	$4.07 \times 10^{-6}$	0.839	$1.35 \times 10^5$

3.5.2 EIS of X70 steel at exposure time of 35 d

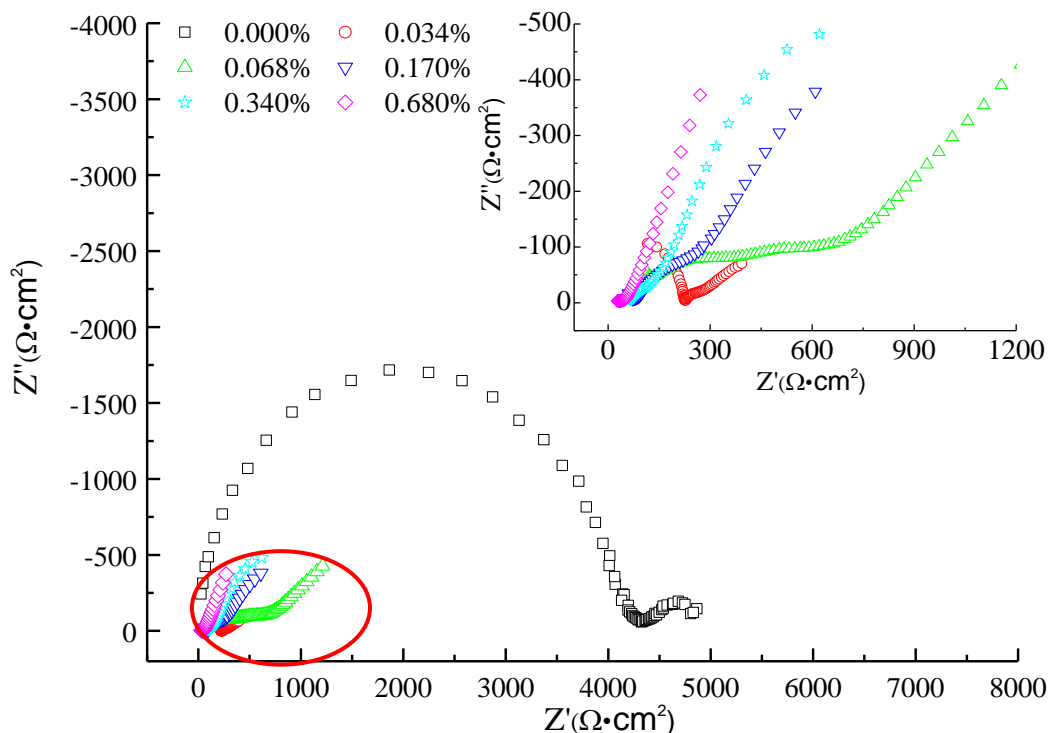


**Figure 12.** EIS of X70 steel in contaminated sand soil with different zinc (II) content at exposure time of 35d: 0.000%, 0.034%, 0.068%, 0.170%, 0.340%, and 0.680%.

Figure 12 shows EIS data of X70 embedded in different sand soil samples contaminated by zinc (II) for 35 d. It was concluded that in non/low-contaminated sand soil, the EIS data of X70 steel

at exposure time of 35 d is similar with those data at exposure time of 7 d, which consist of two capacitive arcs that correspond to ( $Q_sR_s$ ) for the sand layer at high frequency and ( $Q_{dl}R_{ct}$ ) at low frequency [45, 46]. However, with an increase in zinc (II) content, the EIS results present a capacitive arc and a line with an approximate  $45^\circ$  angle, which indicates that the diffusion process is an important control step in the electrode process [36]. This result can be explained by the change in sand layer due to the addition of zinc (II) and the corrosion reaction process. Additionally, the EIS data of X70 in non-contaminated sand soil was fitted by the equivalent circuit in Figure 13A, whereas the EIS data of X70 in zinc (II)-contaminated sand soil were fitted by the equivalent circuit in Figure 13B. The results are also shown in Figure 14 and Table 6. Similarly, the resistance of the electrolyte solution ( $R_l$ ) is not discussed;  $Q_s$  is the capacitance of the sand layer;  $R_s$  is the resistance of the sand layer;  $Q_{dl}$  is the capacitance of the double layer;  $R_{ct}$  is the charge transfer resistance; and  $W$  is the Warburg impedance. The results also show that the addition of zinc (II) contamination in sand soil accelerated the mass transfer process of the electrolyte, and hence the EIS model of metal/sand changed from A to B [45, 46]. However, the change occurred at a low content of zinc (II) contamination in the sand soil (0.034%).

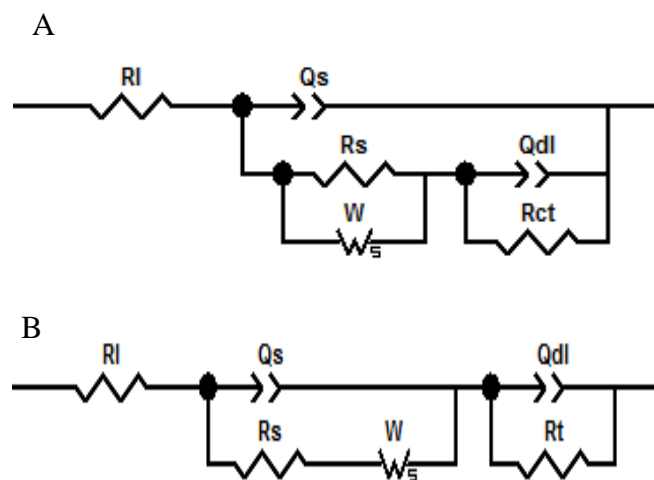


**Figure 13.** Equivalent circuit for low frequency region in EIS of X70 steel in zinc (II) contaminated sand (exposure time of 35d): A, 0.000%; B, 0.034%, 0.068%, 0.170%, 0.340%, 0.680%.

With an increase in zinc (II) content, the magnitude of  $R_{ct}$  substantially fluctuated between  $10^2 \sim 10^3$ , which is attributed to the adsorption and desorption of the corrosion product layer and sand particles on the metal electrode. At a zinc (II) content of 0.680%, the irregular change may be caused by the larger adsorption of the stable corrosion product layer. In addition, the EIS results present typical Warburg diffusion impedance characteristics at exposure time of 35 d, which indicate that the control step of the electrode reaction shifted from activation control to diffusion control [42]. These results can be explained as follows. In a sand medium, the material moved primarily by slow diffusion caused by a concentration gradient. At the beginning of the corrosion process, oxygen from pore water

and air (near the electrode) was sufficient to begin the electrode reaction. The corrosion rate was controlled by electrode activation. As the process of corrosion continued, the diffusion of oxygen to the electrode surface was hindered, and the oxygen was insufficient for the cathodic reaction. The control reaction also changed from an activation to a diffusion reaction. Additionally, more corrosion product coverage on electrode caused by  $Zn^{2+}$  in sand soil further impeded the transmission of oxygen and ions. An increase in salt in the electrolyte also decreased the dissolved oxygen, which further deteriorated the deficiency of oxygen.

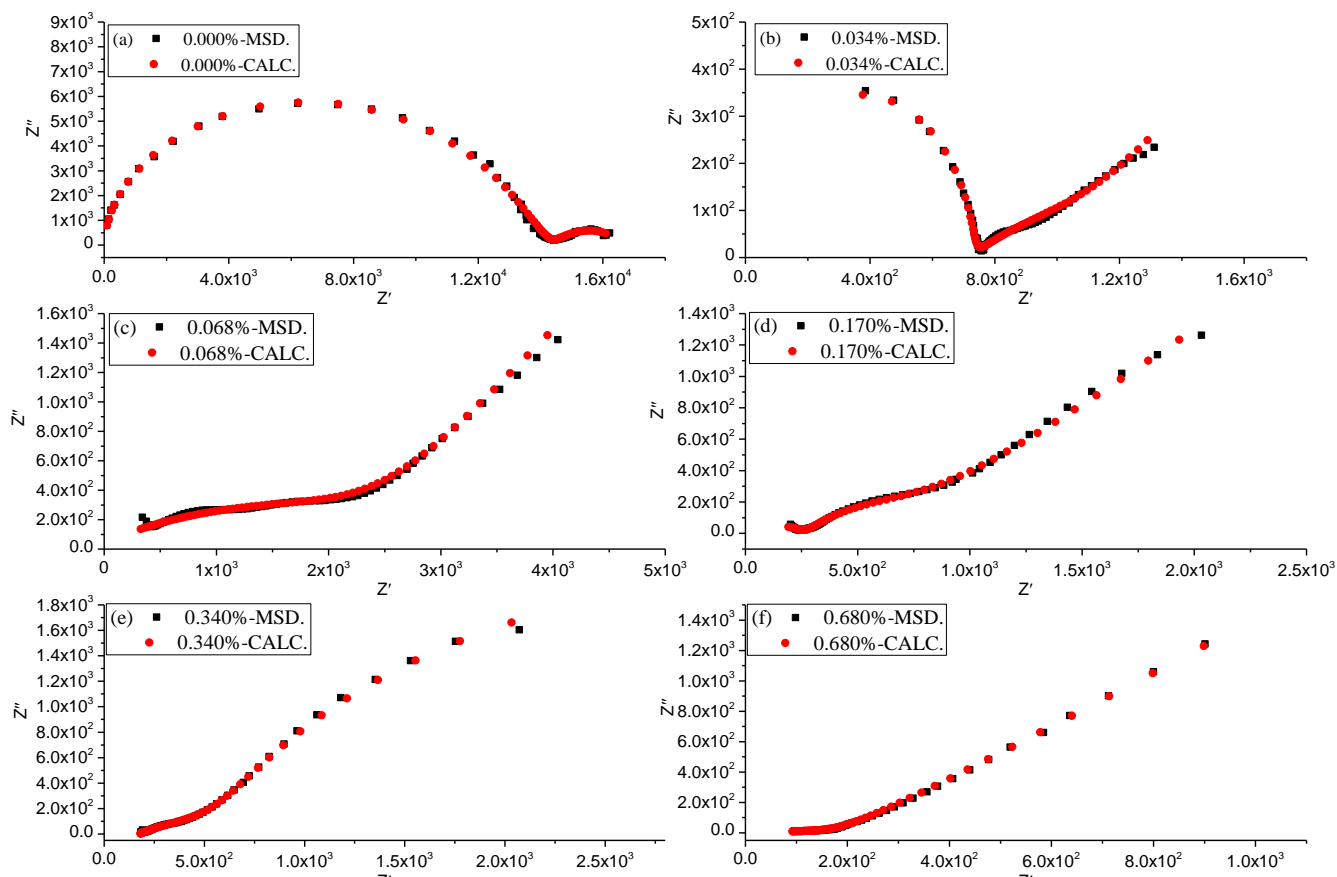


**Figure 14.** Fitted results for EIS of X70 steel in sand soil contaminated by zinc (II) (exposure time of 35 d): (a) 0.000%, (b) 0.034%, (c) 0.068%, (d) 0.170%, (e) 0.340% and (f) 0.680%.

The deviation in the degree of capacitance to an ideal state at exposure time of 35 d was larger than that after 7 d, as shown in Table 7. This may be related to the adherence of corrosion products to the electrode surface, which increased the surface roughness. Additionally, the emergence of corrosion pitting on electrode also changed the surface state. Thus, the value of  $n$  decreased. Moreover, the resistance of charged particles crossing the sand layer and electric double layer both decreased by approximately 1~2 orders of magnitude, which indicates a further destruction of the sand layer and an increase in the corrosion reaction of the metal. The Warburg impedance emerged, and the deviation degree of the electric double layer to an ideal state also increased.

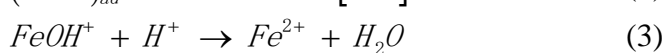
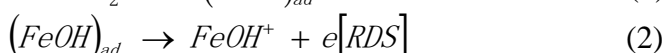
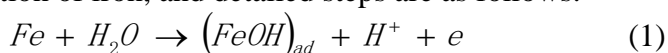
**Table 6.** Fitted results of EIS for X70 steel in sand soil contaminated by zinc (II) (exposure time of 35 d)

$C_{\text{zinc(II)}}$ /%	$R_l$ / $\Omega \cdot \text{cm}^2$	$Q_s$		$R_s$ / $\Omega \cdot \text{cm}^2$	$Q_{dl}$		$R_{ct}$ / $\Omega \cdot \text{cm}^2$	$Y_w$ / $S^{-0.5} \cdot \Omega \cdot \text{cm}^{-2}$
		$Q_s - Y_0$ / $\Omega^{-1} \cdot \text{cm}^{-2} \cdot s^{-n}$	$Q_s - n$		$Q_{dl} - Y_0$ / $\Omega^{-1} \cdot \text{cm}^{-2} \cdot s^{-n}$	$Q_{dl} - n$		
0.000	$4.17 \times 10^{-2}$	$1.61 \times 10^{-9}$	1.00	$1.45 \times 10^4$	$9.11 \times 10^{-4}$	0.59	$2.27 \times 10^3$	$1.26 \times 10^{-7}$
0.034	$1.28 \times 10^{-2}$	$1.93 \times 10^{-3}$	0.31	$8.65 \times 10^2$	$2.94 \times 10^{-9}$	0.97	$7.21 \times 10^2$	$5.59 \times 10^{-3}$
0.068	$2.28 \times 10^{-2}$	$4.69 \times 10^{-9}$	1.00	$1.81 \times 10^2$	$6.26 \times 10^{-5}$	0.31	$2.34 \times 10^3$	$1.64 \times 10^{-3}$
0.170	$9.37 \times 10^{-4}$	$5.74 \times 10^{-6}$	0.42	$2.73 \times 10^2$	$4.66 \times 10^{-4}$	0.58	$4.59 \times 10^2$	$2.05 \times 10^{-3}$
0.340	$1.76 \times 10^2$	$2.97 \times 10^{-3}$	0.84	$3.98 \times 10^3$	$9.36 \times 10^{-4}$	0.37	$6.32 \times 10^2$	$4.65 \times 10^{-3}$
0.680	$4.62 \times 10^{-5}$	$4.67 \times 10^{-3}$	0.06	$3.59 \times 10^2$	$3.50 \times 10^{-3}$	0.68	$2.6 \times 10^{13}$	$6.49 \times 10^{-12}$

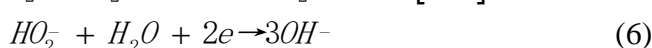
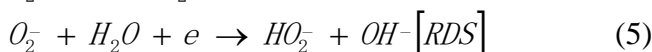
**Table 7.** Fitted results for EIS of X70 steel in zinc (II) contaminated sand (exposure times of 7 d and 35 d)

$C_{\text{zinc(II)}}$ (%)	$R_{ct}$ ( $\Omega \cdot \text{cm}^2$ )		$R_s$ ( $\Omega \cdot \text{cm}^2$ )		$Q_{dl} - n$	
	7 d	35 d	7 d	35 d	7 d	35 d
0.000	$1.91 \times 10^5$	$2.27 \times 10^3$	$1.90 \times 10^5$	$1.45 \times 10^4$	0.741	0.59
0.034	$8.63 \times 10^4$	$7.21 \times 10^2$	$1.22 \times 10^4$	$8.65 \times 10^2$	0.712	0.97
0.068	$4.80 \times 10^4$	$2.34 \times 10^3$	$8.11 \times 10^3$	$1.81 \times 10^2$	0.776	0.31
0.170	$1.51 \times 10^5$	$4.59 \times 10^2$	$3.05 \times 10^3$	$2.73 \times 10^2$	0.698	0.58
0.340	$1.08 \times 10^5$	$6.32 \times 10^2$	$2.69 \times 10^3$	$3.98 \times 10^3$	0.735	0.37
0.680	$1.35 \times 10^5$	$2.63 \times 10^{13}$	$2.65 \times 10^4$	$3.59 \times 10^2$	0.839	0.68

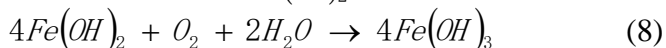
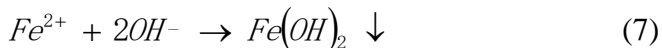
In terms of the corrosion mechanism, the corrosion process of X70 steel consisted of one anodic reaction and one cathodic reaction in non-contaminated sand soil. The anodic reaction was the dissolution of iron, and detailed steps are as follows:



Amongst them, (2) is the control step (RDS) of anodic reactions, and the subscript *ad* indicates the adsorption state. The cathodic reaction was the reduction of oxygen:



Step (5) was the control step (RDS) of the cathodic reactions. In addition, the secondary reaction between the cathodic product of  $\text{OH}^-$  and anodic product of  $\text{Fe}^{2+}$  occurred under the influence of a concentration difference as follows:

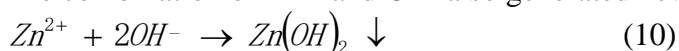


Then, iron hydroxide continuously dispersed into a variety of iron oxides under the action of oxygen.

In zinc (II)-contaminated sand soil, the corrosion process of X70 steel was consistent with one anodic reaction and two cathodic reactions due to the hydrolysis of zinc ions. The hydrogen evolution reaction is a new cathodic reaction that is based on the above corrosion process, which is as follows:



The combination of  $\text{Zn}^{2+}$  and  $\text{OH}^-$  also generated new corrosion products.



#### 4. CONCLUSIONS

This work demonstrated that zinc (II) significantly affects the corrosion behaviour of X70 steel exposed in zinc (II)-contaminated sand soil for 7 d and 35 d, which is different from that what was observed with chloride ion- and carbonate/bicarbonate-contaminated soil. Generally, the addition of zinc (II) in sand soil accelerated the corrosion of X70 steel based on the protection of corrosion products on the electrode. Below, the following conclusions are summarized.

(1). The corrosion of X70 steel in non/low-contaminated sand soil ( $C_{\text{zinc (II)}} \leq 0.034\%$ ) was a localized corrosion process. In high-contaminated sand soil ( $C_{\text{zinc (II)}} = 0.068\% - 0.680\%$ ), the corrosion of X70 steel exhibited an uneven general corrosion process. Additionally, in contaminated sand soil, the corrosion degree of X70 was the most severe at a zinc (II) content of 0.034%. The combined dissolution of iron in the anodic region and the reduction of oxygen and hydrogen in cathodic region led to electrode corrosion in the contaminated sand soil.

(2). The corrosion products of X70 steel in non-contaminated sand soil were mainly composed of  $\text{Fe}_2\text{O}_3$  and  $\text{FeOOH}$ , whereas those in zinc (II)-contaminated sand soil were composed of inner layer iron-containing compounds and outer layer zinc-containing compounds. Moreover, the addition of Zinc (II) in sand soil increased the coverage degree and diversification of corrosion products, such as needle-like and scaly corrosion products presented in corrosion pits.

(3). The zinc (II) contaminated sand soil accelerated the corrosion of X70 steel, especially with a high content of zinc (II). Thus, the corrosion of X70 steel is still severe under a content of 0.034% and exposure time of 35 d. At exposure time of 7 d, the corrosion rate first increased, then decreased and next increased with increasing zinc (II) in sand soil, and the maximum and minimum values were acquired at zinc (II) contents of 0.068% and 0.170%, respectively. At exposure time of 35 d, the corrosion rate increased, then decreased and later approached a stable rate with an increase in zinc (II) in sand soil. The maximum value was acquired at a zinc (II) content of 0.034%.

(4). In non-contaminated soil, the EIS data for X70 steel at exposure times of 7 d and 35 d both consisted of two capacitive arcs. Additionally, both arcs decreased as the corrosion progressed. In zinc

(II)-contaminated sand soil, the EIS data of X70 steel at exposure time of 7 d consisted of an incomplete capacitance arc (high frequency), a capacitive arc (mid-low frequency) and an inductive arc (low frequency), whereas the EIS data of X70 steel at exposure time of 35 d consisted of an incomplete capacitance arc (high frequency) and a Warburg impedance (low frequency).

The corrosion mechanism of X70 steel in sand soil contaminated by zinc (II) changed with time and zinc (II) content, which is conducive to the control of soil corrosion for X70 steel and provides a theoretical basis for future research.

#### ACKNOWLEDGEMENTS

This work was supported by National Natural Science Foundation of China (No. 51208333 and 51501125), China Postdoctoral Science Foundation (No. 2016M591415), Natural Science Foundation of Shanxi Province (No.2013021013-2, No.2014011036-1, No. 2014131019), Program for the Outstanding Innovative Teams of Higher Learning Institutions of Shanxi (No.OIT2015), Program for State Key Laboratory of Hydraulic Engineering Simulation and Safety of Tianjin University (HESS1613).

#### References

1. A. C. Tobón, M. D. Cruz, J. L. G. Velázquez and J. G. G. Salcedo, *Int. J. Electrochem. Sci.*, 9 (2014) 2254.
2. W. Tian, W. H. Yu, N. M. Lin, J. J. Zou, J. W. Guo, H. Y. Zhang, P. Zhou, R. Z. Xie, Y. Ma, Z. X. Wang, X. F. Yao, P. J. Han, X. P. Liu and B. Tang, *Int. J. Electrochem. Sci.*, 10 (2015) 6057.
3. N. M. Lin, F. Q. Xie and B. Tang, *Rare Metal Mat Eng*, 41 (2012) 658.
4. N. M. Lin, P. Zhou, Y. T. Wang, J. J. Zou, Y. Ma, Z. X. Wang, W. Tian, X. F. Yao and B. Tang, *Surf. Rev. Lett.*, 22 (2015) 1.
5. N. M. Lin, P. Zhou, H. W. Zhou, J. W. Guo, J. J. Zou, W. Tian, X. F. Yao and B. Tang, *kovove mater.*, 53 (2015) 147.
6. N. M. Lin, M. L. Li, J. J. Zou, X. G. Wang and B. Tang, *J. Mater. Eng. Perform.*, 22 (2012) 1365.
7. N. M. Lin, P. Zhou, J. J. Zou, F. Q. Xie and B. Tang, *J. Wuhan Univ. Technol.*, 30 (2015) 622.
8. F. P. Mo and F. Cheng, *Min. Resour. Geol.*, 29 (2015) 114.
9. Z. Z. Song, *Shanxi Archit.*, 42 (2016) 91.
10. C. F. Chu, F. S. Zha, L. Xia and L. B. Wang, *Ind. Constr.*, 45 (2015) 118.
11. Z. Z. Liang, S. W. Qi and Q. H. He, *Tianjin Agric. Sci.*, 22 (2016) 5.
12. M. Ye, T. Li, L. P. Xu and R. Wang, *J. Civil, Archit. & Environ. Eng.*, 38 suppl. (2016) 135.
13. M. Taghipour, G. R. Lashkaripour, M. Ghafoori and N. Hafezimoghaddas, *Anti-corros. Methods Mate.*, 63/5 (2016) 347.
14. M. R. Dafter, *Corros. Sci. Technol.*, 15 (2016) 217.
15. S. A. Miran, Q. D. Huang and H. Castaneda, *J. Infrastruct. Syst.*, 22 (2016) 1.
16. Y. Sahraoui and A. Chateaneuf, *Int. J. Press. Vessels Pip.*, 146 (2016) 188.
17. R. Akkouche, C. Remazeilles, M. Jeannin, M. Barbalat, R. Sabot and Ph. Refait, *Electrochim. Acta*, 213 (2016) 698.
18. G. Q. Yin, L. H. Zhang, S. W. Chang and E. H. Han, *Corros. Sci. Prot. Technol.*, 16 (2004) 367.
19. D. C. Feng, Y. Q. Song, T. Li and X. G. Li, *Corros. Sci. Prot. Technol.*, 23 (2011) 78.
20. W. W. Zhang, Q. W. Cai, H. B. Wu and Y. Ren, *Corros. Prot.*, 29 (2008) 368.
21. X. L. Ning, Q. H. Min, C. Wei, Z. Lei, L. M. Xu and L. S. Fei, *J. Univ. Sci. Technol. Beijing*, 33 (2011) 1478.
22. Y. Yang, Z. L. Li and C. Wen, *Corros. Prot.*, 34 (2013) 391.
23. M. X. Li, R. Wang and Z. Q. Bai, *Corros. Sci. Prot. Technol.*, 16 (2004) 17.

24. X. W. Xie, J. Wang, T. Li and Y. Q. Song, *J. Inner Mongolia Univ. Sci. Technol.*, 27 (2008) 307.
25. L. Zhang, X. G. Li, C. W. Du, Z. Y. Liu and P. Liang, *Acta Metall. Sinica*, 44 (2008) 1439.
26. H. Y. Li, W. Kang, J. D. Hu and Y. Liu, *Trans. Mater. Heat Treat.*, 32 (2011) 151.
27. Y. H. Wu, C. Sun, S. Q. Zhang, D. C. Cai, G. H. Li and X. Liu, *Corros. Sci. Prot. Technol.*, 17 (2005) 87.
28. L. C. Zhao, C. Sun, F. B. Zhang and D. C. Cai, *Corros. Sci. Prot. Technol.*, 19 (2007) 27.
29. B. He, C. H. Lu, P. J. Han and X. H. Bai, *Mater. Corros.*, 59 (2016) 418.
30. B. He, P. J. Han, C. Lu and X. H. Bai, *Materialwiss. Werkst.*, 46 (2015) 1077.
31. J. C. Yang, L. J. Zuo, B. X. Zhao and Y. L. Nie, *Spec. Steel*, 33 (2012) 49.
32. H. Y. Wang, X. X. Xu, C. W. Du, Z. S. Xia and X. H. Li, *Henan Metall.*, 19 (2011) 26.
33. J. G. Wang, X. Y. Li and Y. Gao, *Chin. Pet. Mach.*, 42 (2014) 113.
34. Z. Y. Liu, X. Z. Wang, C. W. Du, J. K. Li and X. G. Li, *Mater. Sci. Eng. A*, 658 (2016) 348.
35. X. Wang, H. M. Wu, D. Hou, H. G. Li and L. S. Yu, *Corros. & Prot.*, 35 (2014) 1087.
36. M. R. O. Vega, S. R. Kunst, J. A. T. da Silva, S. Mattedi and C. de Fraga Malfatti, *Corros. Eng. Sci. Technol.*, 50 (2015) 547.
37. P. J. Han, R. Z. Xie, N. M. Lin and B. He, *Int J Electrochem Sci.*, 11 (2016) 9491.
38. B. C. Wang, *Corrosion and Protection of Materials*, Peking University Press, (2012) Beijing, China.
39. Z. Y. Cui, Z. Y. Liu, X. Z. Wang, Q. Li, C. W. Du, X. G. Li and W. Zhang, *Corros. Eng., Sci. Technol.*, 51 (2016) 352.
40. A. Torres-Islas and J. G. González-Rodríguez, *Int J Electrochem Sci.*, 4 (2009) 640.
41. S. R. Wang, *J. Mech. Eng.*, 51(2015) 30.
42. H.Y. Tang, G. L. Song, C. N. Cao and H. C. Lin, *Corros. Sci. Prot. Technol.*, 7 (1995) 285.
43. N. M. Lin, X. B. Huang, X. Y. Zhang, A. L. Fan, L. Qin and B. Tang, *Appl. Surf. Sci.*, 258 (2012) 7047.
44. H.Y. Tang, G. L. Song, C. N. Cao and H. C. Lin, *Corros. Sci. Prot. Technol.*, 8 (1996) 179.
45. C. N. Cao and J. Q. Zhang, *An Introduction to Electrochemical Impedance Spectroscopy*, Science Press, (2002) Beijing, China.
46. E. Barsoukov and J. Ross Macdonld, *Impedance Spectroscopy, Theory, Experiment, and Applications*, John Wiley & Sons, Inc., (2005) Hoboken, New Jersey.
47. Y. L. Zhang, D. T. Sun, G. L. Guo and L. L. Gui, *Chem. J. Chin. Univ.*, 21 (2000) 1086.